THE JOURNAL OF BIOLOGICAL CHEMISTRY VOL. 291, NO. 48, pp. 25217–25226, November 25, 2016

Modulating the Effects of the Bacterial Chaperonin GroEL on Fibrillogenic Polypeptides through Modification of Domain Hinge Architecture*

Received for publication, August 4, 2016, and in revised form, October 5, 2016 Published, JBC Papers in Press, October 14, 2016, DOI 10.1074/jbc.M116.751925

Naoya Fukui[‡], **Kiho Araki**[‡], **Kunihiro Hongo**[‡§], **Tomohiro Mizobata**[‡§], **and Yasushi Kawata**[‡§1]

From the [‡]*Department of Chemistry and Biotechnology, Graduate School of Engineering, and the* [§]*Department of Biomedical Science, Institute of Regenerative Medicine and Biofunction, Graduate School of Medical Science, Tottori University, Tottori 680-8552, Japan*

Edited by Paul Fraser

The isolated apical domain of the *Escherichia coli* GroEL subunit displays the ability to suppress the irreversible fibrillation of numerous amyloid-forming polypeptides. In previous experiments, we have shown that mutating Gly-192 (located at hinge II that connects the apical domain and the intermediate domain) to a tryptophan results in an inactive chaperonin whose apical domain is disoriented. In this study, we have utilized this disruptive effect of Gly-192 mutation to our advantage, by substituting this residue with amino acid residues of varying van der Waals volumes with the intent to modulate the affinity of GroEL toward fibrillogenic peptides. The affinities of GroEL toward fibrillogenic polypeptides such as Aβ(1–40) (amyloid-β(1–40)) peptide and α-synuclein increased in accordance to the larger van der Waals volume of the substituent amino acid side chain in the G192*X* mutants. When we compared the effects of wild-type GroEL and selected GroEL G192*X* mutants on α-synuclein fibril formation, we found that the effects of the chaperonin on α-synuclein fibrillation were different; the wild-type chaperonin caused changes in both the initial lag phase and the rate of fibril extension, whereas the effects of the G192*X* mutants were more specific toward the nucleus-forming lag phase. The chaperonins also displayed differential effects on α-synuclein fibril morphology, suggesting that through mutation of Gly-192, we may induce changes to the intermolecular affinities between GroEL and α-synuclein, leading to more efficient fibril suppression, and in specific cases, modulation of fibril morphology.

Chaperonins are well preserved complex oligomeric systems whose cellular role is to suppress the irreversible aggregation of various proteins in a typical cell and promote refolding and recovery of biological activity (1). The general mechanism of chaperonin action, exemplified in the GroE system from *Escherichia coli*, consists of the recognition and binding of denatured, aggregation-prone protein molecules via hydrophobic interactions (mediated by the apical domain of the GroEL subunit), followed by the binding of nucleotide ATP, which triggers the binding of the co-chaperonin GroES and dynamic movements of the GroEL subunit that internalize the bound protein molecule into the characteristic central cavity of the unique, double-ringed quaternary structure of the GroEL tetradecamer (2). Subsequent hydrolysis of ATP acts as a timer that regulates the interval during which the internalized molecule remains within the central cavity. The protein is then released from GroEL, either having modified its original structure autonomously so that the risk of aggregation is lessened, or according to alternative views, having undergone an active rearrangement of its structure through GroEL to "rewind" the molecule for another attempt at correct folding (3, 4). Bacterial chaperonins such as GroE are known to apply this general mechanism of protein folding assistance to proteins regardless of their source or biological activity. The effects of GroE are partially limited, however, by a molecular size criterion that determines whether a given protein is able to be internalized within the central cavity of GroEL (5).

Recent advances in understanding cellular protein homeostasis have indicated that under certain conditions, cellular proteins form fibrillar protein deposits, which are in turn implicated in various molecular diseases (6–12). These protein fibrils typically evolve very slowly over a long interval within certain cells to form insoluble, characteristically fibrous deposits that may be identified pathologically. It has been shown that various molecular chaperones that are normally present in the cell interact with these proteins that are prone to long-term aggregation and deposition, and partially control or prevent this deposition from occurring (13–17). The interactions between fibrillogenic proteins and molecular chaperones may extend toward molecular chaperones from bacterial origins (18–20). In our experiments, we have found that the isolated apical domain of GroEL (spanning residues 191–376 of the original GroEL subunit) is capable of suppressing the fibrillation of polypeptides such as Aβ(1–42),[2] α-synuclein (αSyn),

* This work was supported in part by Grant-in-Aid for Scientific Research (C) 25440027 from the Japan Society for the Promotion of Science (JSPS) and Grant-in-Aid for Scientific Research on Innovative Areas 2411376 from the Ministry of Education, Culture, Sports, Science and Technology (MEXT). This research was also partially supported by the Strategic Research Program for Brain Sciences from Japan Agency for Medical Research and Development (AMED). The authors declare that they have no conflicts of interest with the contents of this article.

[1] To whom correspondence should be addressed: Dept. of Chemistry and Biotechnology, Graduate School of Engineering, Tottori University, Koyama-Minami, Tottori 680-8552, Japan. Fax: 81-857-31-0881; E-mail: kawata@bio.tottori-u.ac.jp.

[2] The abbreviations used are: Aβ, amyloid-β; ANS, 1-anilinonaphthalene-8-sulfonate; αSyn, α-synuclein; MDH, malate dehydrogenase; QCM, quartz crystal microbalance; Th-T, thioflavin-T; TEM, transmission electron microscopy.

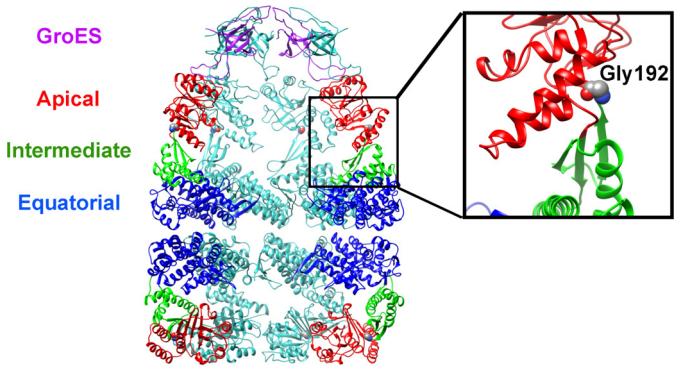

FIGURE 1. **Structural model of GroE, showing the location of Gly-192 in the GroEL subunit.** The figure on the *left* is a cutaway image of the $GroEL_{14}$·ADP_7·$GroES_7$ complex, derived from Protein Data Bank (PDB) file 1AON (36). Selected GroEL and GroES subunits have been removed to showcase the characteristic central cavity of $GroEL_{14}$. The GroEL subunits shown in the forefront of the figure have been colored to highlight the domain architecture; the apical domain is in *red*, the intermediate domain is in *green*, and the equatorial domain is in *blue*. The panel on the *right* is an expanded view of the hinge II region of the GroEL subunit, with Gly-192 represented as space-filling forms. Images were drawn using UCSF Chimera (37).

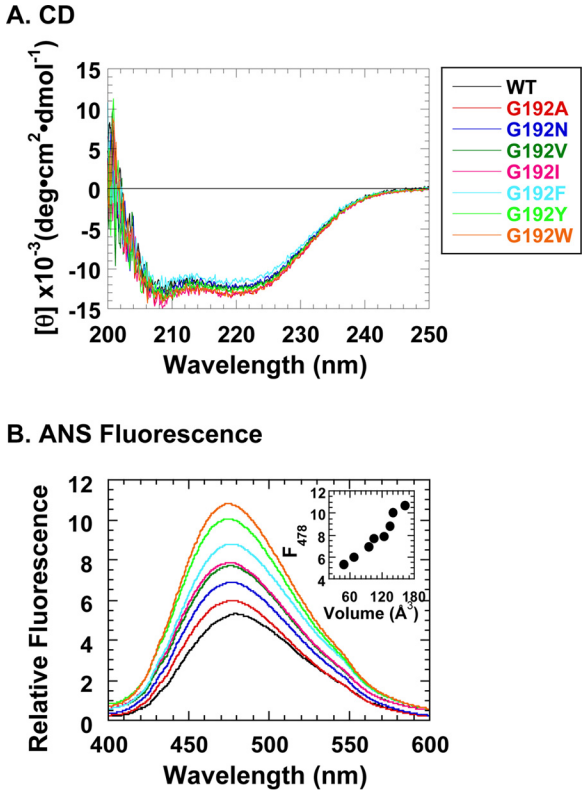

FIGURE 2. **Structural characterization of the seven GroEL G192*X* mutants.** *A*, far-UV CD spectra of GroEL mutants. The *color legend* next to *panel A* denotes the data corresponding to each mutant, and this legend is valid, when applicable, for the data in each panel shown in Figs. 2–4. *B*, ANS fluorescence spectra of GroEL mutants to gauge surface hydrophobicity. The *inset* in *B* is a plot of the fluorescence intensity at 478 nm (F_{478}) for each trace against the van der Waals volume of the amino acid side chains that replace Gly-192 in each mutant.

and GroES (21). Through understanding the underlying principles by which various molecular chaperones interact with fibril-forming polypeptides, it may become possible to develop agents that suppress the irreversible fibrillation of proteins that are conducive to numerous diseases.

During the course of our studies on the GroEL subunit, we characterized a point mutation (G192W) with unique characteristics (22). Gly-192 is located within a hinge region that connects the apical domain and the intermediate domains of GroEL, and this hinge region is proposed to facilitate the dynamic movement of the apical domain in response to ATP binding and hydrolysis within the GroEL subunit (Fig. 1). Substituting Gly-192 with a bulky tryptophan residue served to hinder this dynamic movement in an unusual manner; the mutant chaperonin displayed the ability to bind the co-chaperonin GroES and unfolded peptide simultaneously, in the marked absence of added ATP (22). Further characterization determined that the apical domain in this mutant was tilted relative to the original subunit configuration in such a manner that the binding of GroES and unfolded polypeptide to the same GroEL 14-mer was now possible. The altered configuration resulted in the display of binding interfaces that were hidden in the wild-type subunit when ATP was not bound.

Taking the unique characteristics of GroEL G192W together with the interesting ability that the GroEL apical domain had shown with regard to protein fibril suppression, we reasoned that it may be possible to engineer an enhanced suppressor of protein fibrillation using the GroEL quaternary structure as a scaffold. To prove our ideas, in this study, we substituted Gly-192 with a number of amino acid residues that differ in the van der Waals volume of their side chains, and then characterized their abilities toward suppressing the aggregation and fibrillation of proteins. We found that, in agreement with our initial expectations, the relative affinities of various GroEL G192*X* mutants toward unfolded peptide and GroES in the absence of ATP could be modulated in accordance with the size of the side chain of the *X*-substituent. This modulation was accompanied by corresponding increases in the surface hydrophobicity of each GroEL mutant. A clear correlation could be observed between the van der Waals volume of various amino acid side chains and the relative affinities of the resultant mutants toward proteins and peptides such as αSyn and Aβ(1–40) peptide. The abilities of the various mutants in suppressing protein fibrillation also showed a strong correlation; the most bulky mutant (G192W) proved to be the most effective suppressor of fibrillation in *in vitro* assays using fluorescence to detect fibril maturation. An unexpected additional finding was that, in addition to this enhanced ability to suppress fibril formation, we could observe changes in the morphology of resultant protein fibrils that formed in the presence of different GroEL variants. Our results suggest that, through adjustment of the orientation of the GroEL apical domain by mutation of Gly-192, it is possible to engineer a series of chaperonins that are capable of modulating the length and shape of protein fibrils. These chaperonins act by interacting with fibrillogenic proteins and their products at multiple points of the fibrillation process.

Results

Fig. 2 shows the results of the initial structural characterization of seven GroEL G192*X* mutants using circular dichroism (CD, Fig. 2*A*) and surface hydrophobicity analysis using the fluorescent probe 1-anilinonaphthalene-8-sulfonate (ANS; Fig. 2*B*). Fig. 3 shows the corresponding functional characteriza-

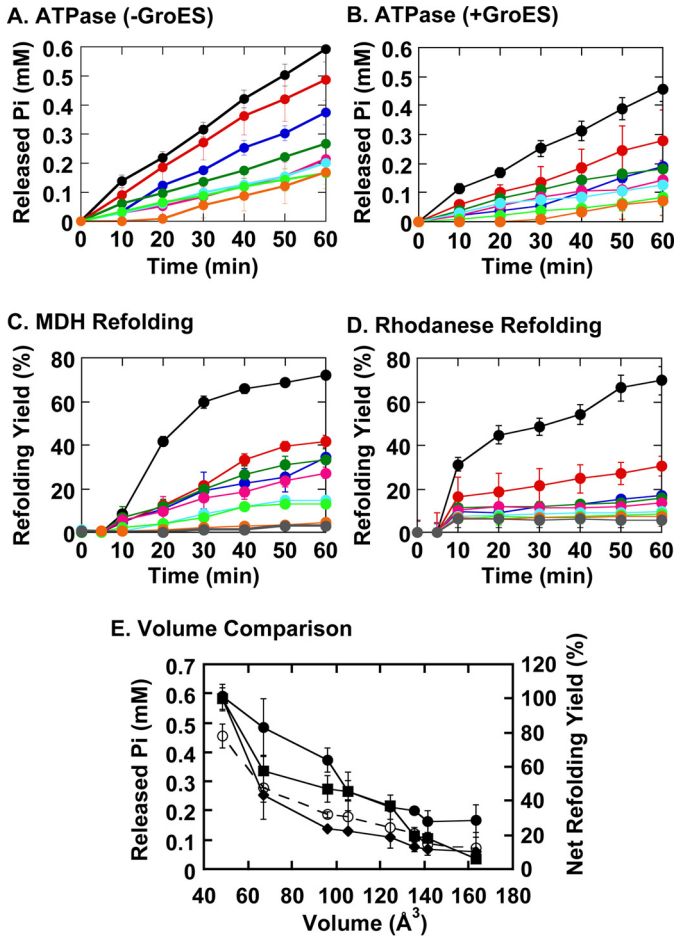

FIGURE 3. **Functional characterization of the seven GroEL G192*X* mutants.** *A*, ATPase activities of the GroEL G192*X* mutants in the absence of GroES. *B*, ATPase activities of the GroEL G192*X* mutants in the presence of GroES. *C*, refolding assays of porcine MDH. *D*, refolding assays of bovine rhodanese. The *gray traces* in *panels C* and *D* denote spontaneous refolding reactions of each substrate protein performed in the absence of chaperonin. Refolding reactions in *panels C* and *D* were initiated in the absence of ATP, and 2 mM ATP was subsequently added at $t = 5$ min. *E*, functional characterizations of the G192*X* mutants summarized by plotting four distinct experimental values: the released inorganic phosphate concentrations detected at $t = 60$ min in *panel A* (*closed circles: solid lines*), similar values for *panel B* (*open circles: dashed lines*), and the net refolding yields at $t = 60$ min shown in *panels C* (*closed squares*) and *D* (*closed diamonds*), in a manner analogous to that shown in the *inset* to Fig. 2*B*. *Error bars* represent the S.E. of each data point.

tions of these mutants using ATPase assays (Fig. 3, *A* and *B*), as well as refolding assays using malate dehydrogenase (MDH) (Fig. 3*C*) and rhodanese (Fig. 3*D*). Fig. 3*E* summarizes our functional evaluations by plotting the net ATPase activities and refolding yields shown in Fig. 3, *A*–*D*, against the van der Waals volumes of the amino acid side chains (23) that replace Gly-192 in each mutant.

The CD spectra of all of the mutants closely resembled the spectra of GroEL WT (Fig. 2*A*), indicating that substitution of Gly-192 with various amino acids resulted in minimal effects on the overall structural integrity of GroEL at the secondary structural level. In contrast, as shown in Fig. 2*B*, substitution of Gly-192 with larger amino acids resulted in a gradual and significant increase in the amount of detected ANS fluorescence. This increase correlated roughly with the size of the amino acid residue that occupied position 192, as demonstrated when we plot the values of the ANS fluorescence intensity at 478 nm (F_{478}) against the side chain van der Waals volumes (23) of each substituting amino acid (Fig. 2*B*, *inset*). We note here that during purification of the mutants, each mutant was eluted from a Superdex 200 Increase gel filtration column at elution volumes (8.75–9.50 ml) that were slightly smaller that of thyroglobulin (M_r 669,000), suggesting that all of the mutants retained the original 14-mer quaternary structure of GroEL.

In Fig. 3, *A* and *B*, the ATPase activities of the various Gly-192 substitution mutants are plotted. We note again a rough correlation between the ATPase activities and the size of the side chain of the amino acid substituent. For each mutant, the addition of GroES to the reaction resulted in a marked decrease in ATPase activity (Fig. 3*E*, compare *closed versus open circles*), indicating that a basic functional relationship between the GroEL ATPase and GroES binding to GroEL (ATPase suppression) was preserved.

With regard to the folding assistance activities of the various mutants (Fig. 3, *C* and *D*), this ability was also affected by the Gly-192 to *X* substitution and also roughly correlated with the size of the side chain that replaced Gly-192. Generally, substituting the glycine at position 192 for amino acids with larger van der Waals volumes resulted in a more severe decrease in folding assistance activity. Some anomalies were apparent: for instance, the strong suppression in MDH refolding assistance abilities in the G192W mutant (Fig. 3*C*, *orange*). Also, regarding rhodanese refolding assistance abilities, we observed that the effects of Gly-192 substitution were more severe, with only G192A displaying a significantly improved refolding yield when compared with the spontaneous reaction (Fig. 3*D*, *red*). Overall, however, the effects of amino acid substitution in Fig. 3 seem to reflect the consequences of steric effects caused by the size of the amino acid substituent, as summarized in Fig. 3*E*.

We next probed the effects of Gly-192 substitution on the binding of the co-chaperonin GroES, through direct quartz crystal microbalance (QCM) analysis. In this assay, we used a concatenated form of GroES where individual subunits were linked by a tri-glycine linker (ESC7) (24) as the binding group immobilized to the sensor and the various GroEL mutants as soluble ligands. The results are summarized in Fig. 4. It should be noted here that, with the exception of the wild-type chaperonin, all of the GroEL mutant proteins were tested for ESC7 binding in the absence of ATP; only GroEL WT was analyzed in both the absence and the presence of 2 mM ATP. As seen in Fig. 4, all of the mutants tested were capable of binding to GroES in the absence of ATP. Generally, a larger van der Waals volume for the substituting mutation corresponded to an increase in $|\Delta F|$, roughly reflecting increased affinities between GroEL and GroES. From the results shown in Fig. 4, we believe that the substitution of Gly-192 with bulkier amino acids served to change the orientation of the apical domain relative to the original closed conformation in the apo GroEL 14-mer, causing an increase in surface hydrophobicity (Fig. 2*B*), an increased affinity toward GroES (Fig. 4), and a decrease in overall "chaperonin competence" (Fig. 3, *C* and *D*).

We next measured the affinities of a selected subset of G192*X* mutants toward two immobilized fibrillogenic polypeptides, Aβ(1–40) peptide and αSyn bound to the sensor via a C-termi-

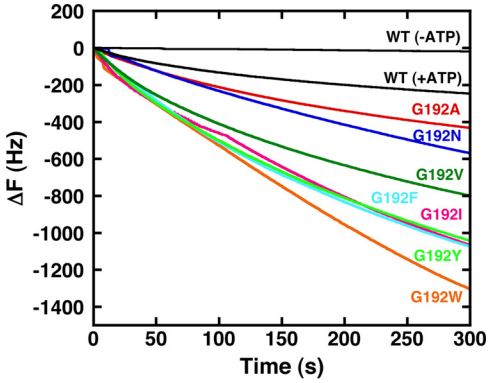

FIGURE 4. **QCM binding analyses of GroEL G192*X* mutants to immobilized GroES ESC7.** Preparations of ESC7 were immobilized to the sensor chip using standard methods, and aliquots of GroEL G192*X* were added to the cell. Signal changes reflect changes to the mass that is bound to the sensor chip, which in this case represents the amount of GroEL G192*X* that is bound to ESC7. With the exception of GroEL WT, all measurements were performed in the absence of ATP.

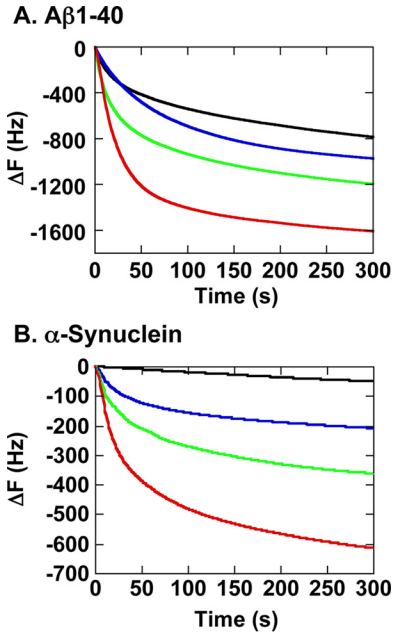

FIGURE 5. **QCM binding analyses of GroEL WT and three G192*X* mutants to immobilized fibrillogenic polypeptides.** *A*, the binding of GroEL to immobilized Aβ(1–40) peptide. *B*, the binding of GroEL to immobilized αSyn-His_6. In each panel, the *black trace* indicates the binding of GroEL WT, the *blue trace* indicates the binding of GroEL G192N, the *green trace* indicates the binding of GroEL G192I, and the *red trace* indicates the binding of GroEL G192W.

nal His_6 tag (αSyn-His_6), using QCM to gauge the effects of the G192*X* mutation on GroEL-Aβ(1–40) and GroEL-αSyn association. For this assay, we selected the mutants G192N, G192I, and G192W. These three mutants, together with GroEL WT, span the range of different affinities that were observed in the GroES binding experiments shown in Fig. 4. As shown in Fig. 5, the G192*X* mutation resulted in changes in the affinities toward GroEL for both immobilized Aβ(1–40) (Fig. 5*A*) and immobilized αSyn-His_6 (Fig. 5*B*). The relationship between the substituting amino acid and the binding affinities was roughly comparable with the changes in affinity toward GroES: GroEL G192W displayed the strongest affinities toward Aβ(1–40) and αSyn-His_6, and GroEL WT displayed the weakest. The results were in line with our explanation that these amino acid substitutions change the orientation of the GroEL apical domain relative to the ring structure, and as a result, structural interfaces that accommodate protein binding are exposed. The finding that the affinities of the G192N mutant and the G192I mutant also fell between wild type and G192W, for both fibrillogenic polypeptides, supported our notion that the size of the substituting residue at position 192 dictates a sliding scale of affinity toward protein ligands.

The interactions between the four selected chaperonins and αSyn-His_6 were probed further by quantitative QCM analysis, and the results are summarized in Fig. 6 and Table 1. We found that the qualitative relationship that we inferred from Fig. 5 was supported in quantitative analyses. Estimated dissociation constants (K_D) of each chaperonin toward immobilized αSyn-His_6 ranged from 8.4×10^{-9} M for G192W to 3.06×10^{-8} M for GroEL wild type (Table 1), again demonstrating a sliding scale of binding affinities correlating with the size of the amino acid side chain that replaces Gly-192.

To determine whether the changes in αSyn-GroEL binding affinities in particular translated to detectable effects in αSyn fibrillogenesis, we next monitored the effects of GroEL G192*X* addition on the time course of αSyn fibril formation using thioflavin-T (Th-T) fluorescence (Fig. 7). As shown in Fig. 7, we found that the addition of either GroEL WT or each of the three G192*X* mutants that we tested indeed caused measurable changes in the time course of αSyn fibrillation. Intriguingly, however, we noted in the experiments a qualitative difference in the effects of GroEL wild-type and the G192*X* mutant chaperonins on αSyn fibrillogenesis. In the case of GroEL WT, the fibrillation profile was altered in a GroEL concentration-dependent manner, but the changes were mainly confined to the rate of fibril extension, with the lag interval remaining relatively unchanged (Fig. 7*A*). In the case of the G192W mutant, however, the addition of increasing amounts of the chaperonin to the reaction caused a specific increase in the lag phase of fibrillation, and the rate of extension as monitored by the slope of Th-T fluorescence increase was relatively constant across the samples. This suggested that this mutant affected most strongly the initial formation of fibril nuclei from which mature fibrils extended (Fig. 7*D*). The effects of the other two mutants lay between these two extremes, and GroEL G192N tended to produce effects that were more pronounced in the fibrillation rate (Fig. 7*B*), whereas GroEL G192I addition caused more drastic changes to the initial lag times (Fig. 7*C*).

Do these varied effects on the fibril extension profile translate into changes in the shape of the fibrils that are eventually formed? To answer this question, we performed transmission electron microscopy (TEM) analysis on fibrils that were formed in the assays shown in Fig. 7 using negative staining. Interestingly, we observed a difference in the morphology of fibrils produced in the presence of these chaperonins (Fig. 8). In the presence of GroEL WT, fibrils tended to develop unbraided, strip-like forms where multiple protofibrils were arranged in parallel, especially at higher ratios of αSyn to GroEL (Fig. 8, see *+WT, x0.2 panel*, bordered in *blue*). In our TEM images, we could also observe particles of GroEL bound to the periphery of

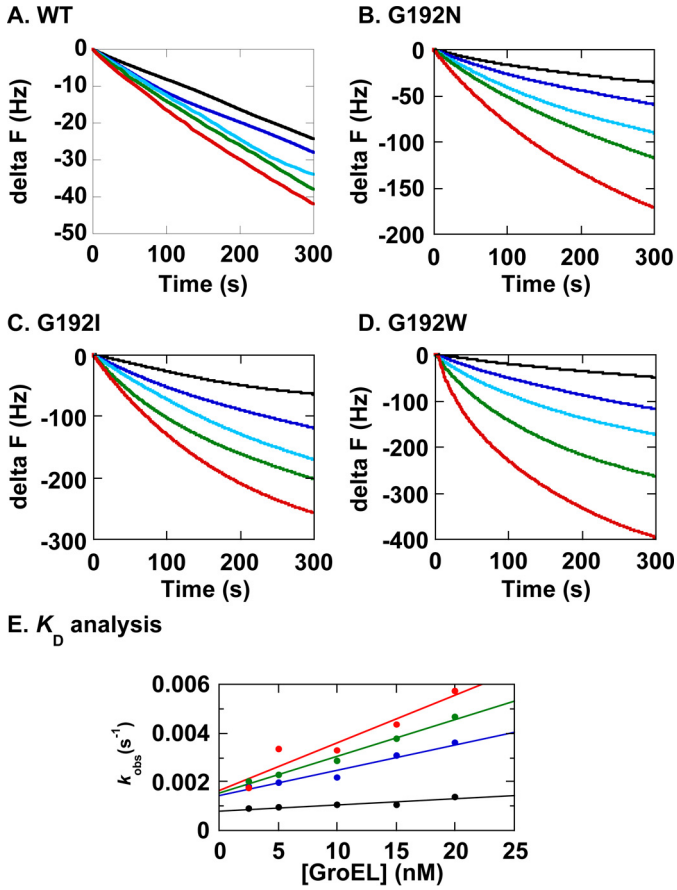

FIGURE 6. **Quantitative QCM binding analyses of GroEL WT and three G192*X* mutants to immobilized αSyn-His$_6$.** *A–D*, titrations of αSyn-His$_6$ immobilized to the QCM sensor with increasing concentrations of GroEL WT (*A*), GroEL G192N (*B*), G192I (*C*), or G192W (*D*). Colors in each panel indicate QCM traces obtained by adding GroEL at the following concentrations: *black*, 2.5 nM; *blue*, 5 nM; *cyan*, 10 nM; *green*, 15 nM; *red*, 20 nM. *E*, estimation of K_D values through linear regression fitting of [GroEL] *versus* k_{obs} plots. *Black*, WT; *blue*, G192N; *green*, G192I; *red*, G192W.

TABLE 1

Summary of the values k_{on}, k_{off}, and K_D, estimated from linear regression analysis of the data shown in Fig. 6*E*

Sample	k_{on}	k_{off}	K_D
	$M^{-1}\,s^{-1}$	s^{-1}	M
WT	2.6×10^4	7.98×10^{-4}	3.06×10^{-8}
G192N	10.5×10^4	14.4×10^{-4}	1.37×10^{-8}
G192I	15.0×10^4	15.5×10^{-4}	1.03×10^{-8}
G192W	19.6×10^4	16.4×10^{-4}	8.4×10^{-9}

the fibrils, reflecting perhaps the persistence of the GroEL-αSyn interactions. In contrast, in the presence of GroEL G192W (Fig. 8, see *+G192W, x0.2 panel*, bordered in *red*), the fibrils observed more closely resembled the braided protofibril forms that are observed when αSyn fibrils are formed in isolation (Fig. 8, *topmost panel*); instead, the fibrils formed were shorter in overall length and were greatly reduced in number. Fibrils that formed in the presence of GroEL G192N and G192I included both parallel oriented forms and shorter, braided forms, as highlighted in Fig. 8 with the corresponding colored borders.

In Fig. 9, we probed the effects of the delayed addition of these chaperonins to the αSyn fibril-forming reaction. The delayed addition of GroEL during αSyn fibrillation resulted in

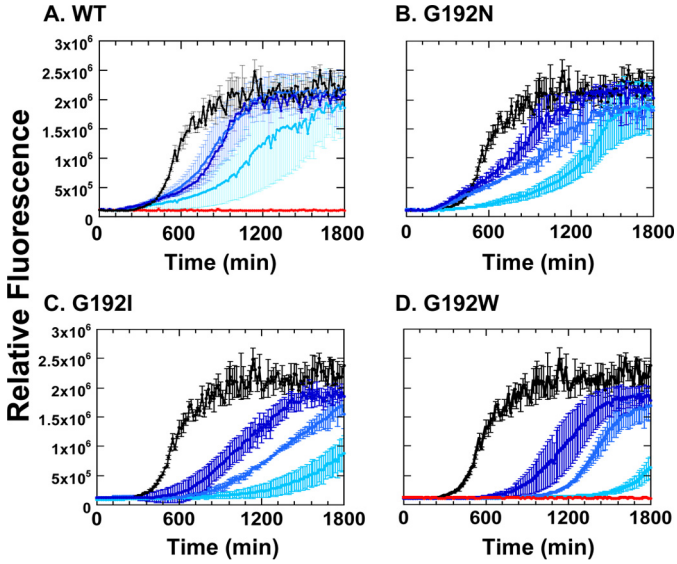

FIGURE 7. **Th-T fluorescence assays of αSyn fibrillation in the presence of GroEL WT and G192*X* mutants.** *A*, GroEL WT. *B*, GroEL G192N. *C*, GroEL G192I. *D*, GroEL G192W. In each panel, *lighter shades of blue* are used to denote increasing concentrations of GroEL added to the experiment. Specific molar ratios of GroEL$_{14}$ added to each sample relative to αSyn monomer are as follows: 0.05:1, 0.1:1, 0.2:1 (from *dark blue* to *light blue*). *Red traces* in *panels A* and *D* indicate Th-T fluorescence changes of GroEL WT and G192W incubated under identical conditions, respectively. *Error bars* represent the S.E. of each data point.

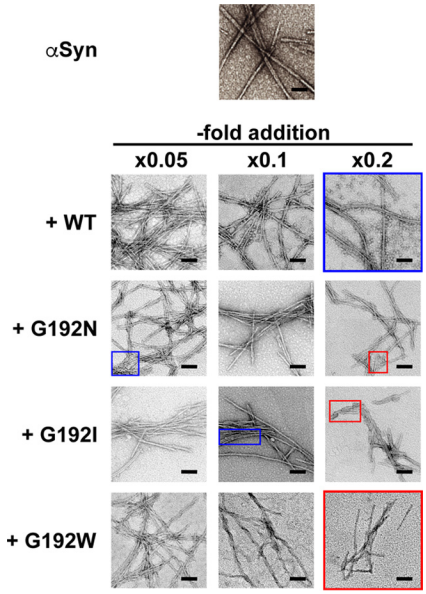

FIGURE 8. **Transmission electron micrographs of αSyn fibrils formed in Fig. 7 (at *t* = 30 h).** *Scale bars* in each panel indicate 100 nm. The *uppermost panel* shows negatively stained samples of typical αSyn fibrils formed in the absence of chaperonin. The *lower panels* are grouped *horizontally* according to the type of chaperonin added to the αSyn fibril-forming reaction, and *vertically* according to the specific ratio of chaperonin oligomer added relative to αSyn monomer. *Blue* and *red borders* indicate grouping of panels and regions that show a common fibril morphology, as discussed in detail under "Results."

changes to the time course of fibrillogenesis. The specific changes that each chaperonin brought about, however, were slightly different between GroEL wild type and the other three GroEL Gly-192 mutants. In the case of GroEL WT, the addition of the chaperonin at different time points of the reaction resulted in changes that varied with the delay before GroEL

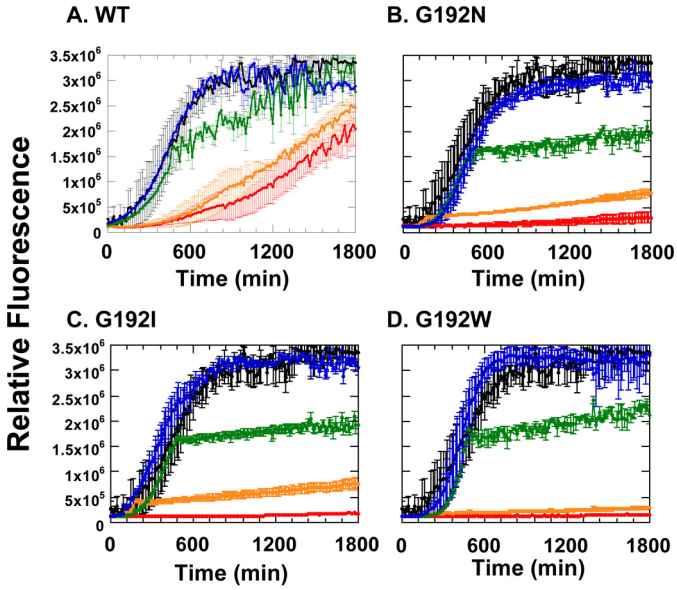

FIGURE 9. **Delayed addition of GroEL WT and G192*X* mutants to fibrillation reactions of αSyn.** *A–D*, after initiating the fibril-forming reaction in the absence of chaperonin, either GroEL WT (*A*) or GroEL G192N (*B*), G192I (*C*), or G192W (*D*) mutant was added after a fixed delay time. The ratio of $GroEL_{14}$ to αSyn added was fixed at 0.2:1. The specific time of delay before the addition of chaperonin to the experiment follows the following convention: *red*, chaperonin added at zero time (no delay); *orange*, chaperonin added after a 3-h (180-min) delay; *green*, chaperonin added after an 8-h (480-min) delay; *blue*, chaperonin added after a 24-h (1440-min) delay. *Black traces* indicate reactions in the absence of chaperonin. *Error bars* represent the S.E. of each data point.

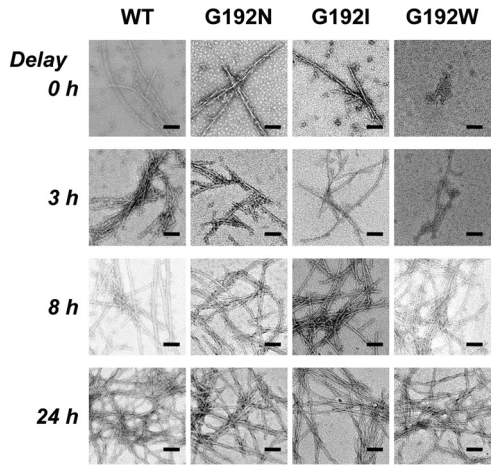

FIGURE 10. **TEM images of αSyn fibril samples that were recovered after the experiments shown in Fig. 9.** Images are grouped *vertically* according to the type of GroEL added. The *top row* indicates αSyn fibrils that formed in the presence of GroEL without delay time (0 h), and subsequent *lower rows* show samples from reactions that were initiated in buffer, with GroEL added at progressively later intervals (3, 8, and 24 h). *Scale bars* indicate 100 nm.

addition (Fig. 9*A*). When GroEL WT was added at the early stages of the fibril-forming reaction (Fig. 9*A*, *red* and *orange*), an elongated lag phase (attributed to fibril nuclei formation) and a decrease in the rate of fluorescence signal increase (attributed to fibril extension) were both observed. Adding GroEL WT to the reaction at later intervals, for example, 8 h after the initiation of the experiment (Fig. 9*A*, *green*), resulted in a decrease in the fibril-forming rate. However, the fluorescence signal increased eventually to values similar to that of samples without added GroEL (Fig. 9*A*, *black*). In contrast, when GroEL G192W was added to the reaction at various time points (Fig. 9*D*), we observed that GroEL G192W was quite effective in immediately halting further fibril formation, even when this chaperonin was added at the midpoint of the extension phase (8 h; Fig. 9*D*, *green*). The affinity of GroEL G192W toward αSyn is higher than the affinity of GroEL WT (Table 1), and this difference in affinities may be causing these differences in additive effect on the αSyn fibril-generating reaction. Reactions where either G192N or G192I was added mimicked the results of GroEL G192W; in each case, delayed addition served to immediately halt further increases in Th-T fluorescence.

When we observed the shape of the fibrils produced in the delayed addition experiments, we were able to confirm the differential effects of GroEL WT and GroEL G192W on the fibril morphology of αSyn that we noted in Fig. 8. As seen in Fig. 10, αSyn fibrils that were formed in samples where GroEL WT was added in the early stages of the fibrillation reaction (0 and 3 h) tended to produce long straight fibrils without twists, confirming the results shown in Fig. 8 that fibrils that formed in the presence of GroEL WT displayed this characteristic morphology. However, this tendency was altered when GroEL WT was added in the latter stages of the reaction; the fibrils produced were much more similar to the braided protofibrils typical of αSyn fibrils formed in isolation (Fig. 10, compare the *topmost* and *bottommost panels* of the *left-side column* denoted *WT*). In contrast, fibrils produced in the presence of GroEL G192W (Fig. 10, *right column*) displayed twisted morphologies irrespective of the time that GroEL was added to the reaction, again confirming the morphological differences of the fibrils that formed in the presence of these two chaperonins, as described in Fig. 8. We may deduce two things from the images in Fig. 10 regarding the effects of GroEL on αSyn fibrillogenesis. First, the effects of the chaperonin on fibril morphology are realized in the initial, early stages of the fibril-forming reaction; GroEL is incapable of altering the morphology of fibrils once they have been formed, because delaying the addition of GroEL to the reaction for 24 h results in the disappearance of all morphological differences between the samples (Fig. 10, *24 h panel*). Second, this ability to change the morphology of αSyn fibrils seems to hinge on the relative affinity that GroEL displays toward αSyn, and this affinity may be modulated by replacing a crucial glycine residue localized in the hinge II region of the GroEL subunit with a bulkier amino acid that tilts the orientation of the GroEL apical domain.

Discussion

Molecular chaperones function as shepherds to various cellular proteins under conditions of stress to maintain the structural integrity and functional abilities of these clients, and also act to smoothly process damaged and inactive proteins through the proteolytic pathway. To achieve these functions, molecular chaperones frequently utilize protein-protein interactions to recognize proteins that are qualified for processing.

Recent *in vivo* studies have highlighted the possibility that, through this protein maintenance activity, various molecular chaperones are actively involved in preventing the accumulation of insoluble, fibrillar protein aggregates that are often

implicated in various cellular diseases. Examples such as the involvement of the small heat shock proteins (14, 25–27), members of the Hsp70 and Hsp104 families (15–17, 28, 29), and the chaperonin/Hsp60 families (30–32) have demonstrated that the involvement of molecular chaperones in the control of protein folding diseases may be a general concept applicable to a variety of phenomena that affect the well being and health of eukaryotic cells.

Building upon this concept, we set out to elucidate general principles that may underlie the control of protein fibrillation by molecular chaperones. We elected to use a model system composed of the bacterial chaperonin GroEL and multiple fibrillogenic proteins. In a previous study, we succeeded in demonstrating that the apical domain of GroEL, which acts as a sensor for proteins susceptible to association and insolubility, is capable of interacting with and suppressing the formation of protein fibrils from various sources (21). The present study is aimed at utilizing and extending our original findings regarding the GroEL apical domain, by revisiting the original chaperonin quaternary structure and selectively modifying a crucial hinge region so that the active apical domain may be reoriented toward our purposes.

Our experiments demonstrated rather clearly that it was indeed possible to modify the structure of the GroEL subunit to enhance its affinity toward fibrillogenic polypeptides, with minimal effects to the overall structural characteristics of the chaperonin. Moreover, the modifications are partially customizable; by substituting Gly-192 with amino acid residues of increasing size, it was possible to gradually increase the affinity of GroEL toward polypeptides such as Aβ(1–40) and αSyn. This increase in affinity was also correlated with an improved ability to suppress the fibrillogenesis of αSyn; the mutant with the bulkiest substitution at position 192 was determined to be the most effective suppressor of αSyn fibrils. The structural basis for this effect seems to be relatively clear-cut; the presence of bulkier amino acid side chains acts to tilt the apical domain to an orientation that exposes more and more of the hydrophobic binding interface for unfolded polypeptide (Fig. 2*B*). We have observed in Machida *et al.* (22) that this is true in the case of GroEL G192W; direct TEM observation showed that in this mutant, the apical domain was tilted in an open-like configuration in the absence of ATP. The additional, interesting finding of the present study was that this effect was adjustable, based upon a sliding scale of the van der Waals volume of the substituting amino acid side chain. It should be relatively easy to build on our results shown here to enhance this ability to even greater levels. Selected modifications to the GroEL apical domain, for example, may conceivably increase the affinity of this domain toward various polypeptides, or lead even to "customized" affinities, where the domain is modified to accommodate only a specific structural motif over other interactions. The findings shown here form a robust platform on which we may build to probe much further the development of protein-based factors that may be utilized in the detection and, ultimately, control of insoluble protein fibrils that are implicated in various protein misfolding diseases.

An additional unexpected and interesting finding was that, in addition to protein fibril suppression, GroEL was also capable of altering the morphology of αSyn fibrils specifically, and this ability was also adjustable by mutating Gly-192. We found that the original GroEL WT, when added to the αSyn fibril-forming reaction at a sufficiently early stage, could change the morphology of αSyn fibrils from its original twisted, braided form to a flat form in which the protofibrils of αSyn are arranged parallel to each other. This fibril-modulating ability may be based on a "loose" interaction with αSyn oligomers or protofibrils, because it was the GroEL variant with the weakest affinity toward αSyn that displayed this tendency. However, specific interactions that are responsible for this ability must be elucidated in further experiments to probe the detailed kinetics of the GroEL-αSyn interaction. Fortunately, however, we already have in our hands a mutant GroEL where this ability has been altered to a more general fibril suppression activity, so a comparative analysis between these two chaperonins, and selected other G192*X* mutants, should provide insights on this interesting effect on fibril morphology.

Experimental Procedures

Preparation of Chaperonins and Client Proteins—Genes encoding the GroEL mutants were constructed by using the QuikChange site-directed mutagenesis kit, using pETEL (pET23a(+)(Novagen)-based plasmid encoding wild-type *groEL*) as the template. The successful construction of each mutant was confirmed by DNA sequence analysis of the entire GroEL coding region. Both wild-type and mutant proteins were expressed in *E. coli* BLR(DE3) and purified at room temperature, using the method described previously (22) involving ammonium sulfate precipitation followed by successive gel filtration (Superdex 200 Increase 10/300 GL) and anion exchange (Resource-Q) chromatography. All chromatography steps were performed on an ÄKTA-FPLC system (GE Healthcare) at room temperature.

MDH from pig heart was obtained commercially from Roche Applied Sciences, and bovine rhodanese was obtained from Sigma-Aldrich and used in refolding studies. Aβ(1–40) peptide was obtained as synthesized peptide from the Peptide Institute (Osaka, Japan). Human αSyn and αSyn-His_6 were each expressed in *E. coli* cells harboring an overproducing plasmid and purified using protocols published in Yagi *et al.* (33).

Buffers—The following buffers were used in this study. Buffer A, 50 mM Tris-HCl buffer, pH 7.8, containing 20 mM KCl, 10 mM $Mg(CH_3COO)_2$, and 2 mM DTT. Buffer B, 30 mM Tris-HCl, pH 7.2, containing 50 mM KCl and 10 mM $Mg(CH_3COO)_2$. Buffer C, 50 mM Tris-HCl, pH 7.5, containing 2 mM EDTA and 2 mM DTT. Buffer D, 20 mM HEPES-NaOH buffer, pH 7.5, containing 150 mM NaCl, 50 mM EDTA, and 10 mM $NiSO_4$. Buffer E, 20 mM HEPES-NaOH, pH 7.5, containing 150 mM NaCl and 0.4 M imidazole. Buffer F, 25 mM Tris-HCl buffer, pH 7.5, containing 150 mM NaCl and 20 μM Th-T (Wako, Osaka, Japan).

Structural Characterization—CD spectra of GroEL mutants (200 μg/ml) were measured in Buffer A. Measurements were performed on a Jasco J-820 spectropolarimeter at 25 °C. Spectra displayed are averages of 10 scans, and corrected for buffer signals. Raw signals were then converted to mean residue ellipticities in Fig. 2*A*.

Fluorescence spectroscopy of GroEL mutants (200 μg/ml) in the presence of ANS was measured on a Jasco FP-6300 fluorescence spectrophotometer in Buffer A containing 5 μM ANS, at an excitation wavelength of 371 nm. Spectra shown are averages of five scans, and buffer contributions were subtracted.

Functional Characterization—ATPase activities of GroEL protein (0.1 μM) in the presence or absence of GroES (0.1 μM) (7-mer) were measured at 37 °C, using a slightly modified protocol of a colorimetric method described previously (34, 35). Experiments were performed in Buffer A. The initial concentration of ATP added was 2 mM, and samples were removed at 10-min intervals to determine the concentration of inorganic phosphate in the assay mixture.

Refolding assays of MDH were carried out as reported previously (22). Refolding of rhodanese was performed using previous protocols. Briefly, purified rhodanese (46 μM) was unfolded in 40 mM Tris-HCl buffer, pH 7.4, containing 6 M guanidine hydrochloride and 1.5 mM DTT at 25 °C for 1 h. The refolding reaction was started by a 100-fold dilution into Buffer B. The temperature and protein concentration of rhodanese during the refolding reaction were 25 °C and 0.46 μM, respectively; a 1.5-fold molar excess of GroEL and GroES oligomer relative to rhodanese was present in the refolding reaction, and 2 mM ATP was added to each reaction at 5 min. The assay was performed at 25 °C.

In both ATPase and refolding assays, the data shown represent averages from three experiments using two independent chaperonin preparations of each variant. Error bars represent the S.E. of each data point. Values for the van der Waals volume of each amino acid side chain that replaced Gly-192 in the mutants were obtained from Darby and Creighton (23) and used to plot the Fig. 2*B inset* as well as Fig. 3*E*.

QCM Assay—An Affinix QNμ (Initium Inc., Japan) QCM instrument was used to directly detect GroEL-protein interactions. The instrument contains one 550-μl cell equipped with a 27-MHz QCM plate (8.7-mm diameter quartz plate and 5.7-mm^2 area gold electrode) at the bottom of the cell and is coupled to a temperature control system. Immobilization of ESC7 and Aβ(1–40) peptide to the sensor cell and subsequent measurements were accomplished utilizing amine coupling as follows. The gold surface of the quartz resonator was first cleaned successively with 1% SDS and piranha solution (H_2SO_4:H_2O_2 = 3:1) prior to immobilization. Carboxyl group-containing self-assembled monolayer (COOH-SAM) reagent was then added to the cleaned gold electrode of the QCM and incubated for 1 h at room temperature. The sensor was washed with Milli-Q water, and the resultant carboxylic groups introduced to the sensor surface were next activated by adding 50 μl of a freshly prepared 1:1 mixture of *N*-hydroxysuccinimide and 1-ethyl-3-(3-dimethylaminopropyl)carbodiimide (50 mg/ml each).

After washing the sensor, 0.5 ml of ESC7 samples (50 μM) in reaction buffer (10 mM citrate buffer, pH 5.0) was added to initiate the binding reaction. This lower pH buffer was necessary to improve the binding of ESC7. For Aβ(1–40), a solution of 5 μM Aβ(1–40) in Buffer B was added to the cell, and binding was allowed to proceed in a similar manner. After monitoring the changes in resonance frequency (ΔF) for a designated interval sufficient for binding, the sample was removed and ethanolamine solution was added to rinse the sensor. The cell was then equilibrated with experimental buffer (Buffer A for ESC7, Buffer B for Aβ(1–40)), followed by the addition of ligand protein solution (containing GroEL mutants) to initiate the assay.

In contrast, immobilization of αSyn-His_6 samples to the sensor was performed using an alternative method involving nickel affinity binding of the C-terminal His_6 tag, to minimize nonspecific interactions between αSyn and the sensor surface. After initializing the sensor chamber by washing the cells with SDS and piranha solution as described above, 100 μl of a solution containing 0.5 mM 3,3′-dithiobis[*N*-(5-amino-5-carboxypentyl)propionamide-*N*′, *N*′-diacetic acid] dihydrochloride (C_2-NTS, Dojindo) was added to the cell and incubated for 10 min at room temperature. This solution was washed away with Milli-Q water, and 500 μl of Buffer D was added and allowed to sit for 10 min at room temperature. Afterward, the cell was again washed with Milli-Q, and then 0.1 μM of αSyn-His_6 in Buffer B was added to the cell. The binding of αSyn-His_6 to the activated sensor was allowed to proceed under observation for 10 min at 25 °C under mixing. Afterward, the cells were washed with Buffer B before adding the respective GroEL samples for the actual measurements in Buffer B. Regeneration of the initial experimental conditions was accomplished after each measurement by washing the sensor cell with Milli-Q, adding 500 μl of Buffer E for 30 min to remove αSyn-His_6, and reapplying Buffer D and fresh αSyn-His_6 solutions, as described above.

In quantitative analyses (Fig. 6*E*), data were analyzed using the software package provided by the manufacturer of the instrument (AQUA 2.0) by linear regression analysis of the observed rate constant (k_{obs}) relative to the concentration of added GroEL G192W mutant, according to the following equation

$$k_{obs} = k_{off} + k_{on}[\text{GroEL}] \quad \text{(Eq. 1)}$$

to estimate k_{off} and k_{on} values, which were subsequently used to estimate the K_D.

Fluorescence Detection of Fibril Maturation using Th-T—Fibril formation of αSyn was monitored using Th-T fluorescence as described in previous studies (21). One milligram per milliliter of αSyn was incubated either alone or in the presence of 2.76 mg/ml GroEL WT or G192*X* mutants at 37 °C in Buffer F. Samples (150 μl) were prepared in triplicate in 96-well plates (8 × 12-well plate; Greiner, Kremsmuenster, Austria) and placed into an ARVO X4 (Perkin Elmer) plate reader that was capable of sustained sample agitation. Increases in Th-T fluorescence were monitored intermittently through the bottom of the plate (read times, 0.1 s; excitation, 440 nm; emission, 486 nm). Data were averaged across the three samples to obtain time-dependent fibrillogenesis traces with TEM.

TEM Analysis—In this study, samples for TEM analysis were obtained from samples measured in Th-T fluorescence assays (Figs. 7 and 9), as described under "Fluorescence Detection of Fibril Maturation using Th-T," with the exception of the control sample of αSyn depicted in Fig. 8. After each fluorescence assay, representative aliquots (10 μl) of each sample were randomly sampled from the wells and applied to carbon-coated 400-mesh copper grids (Nisshin-EM, Tokyo, Japan), and sam-

ple preparation was performed according to the protocol described in Ojha *et al.* (21) using EM Stainer (Nissin-EM, Tokyo). TEM images were obtained using a JEOL JEM-1400Plus transmission electron microscope at 80 kV. For the control αSyn sample in Fig. 8, TEM images were obtained from 2% uranyl acetate-stained samples observed at ×27,000 magnification, with images obtained using a film camera mounted on a JEOL-100CX transmission electron microscope operating at 80 kV. Film negatives were scanned using a commercial flatbed scanner (Canon) at resolutions and sizes that match the resolution and sizes of the digital images obtained for the other samples.

Author Contributions—N. F., T. M., and Y. K. designed the research, and N. F., K. A., and K. H. performed the research. N. F., T. M., and Y. K. wrote the main manuscript text and prepared the figures. All authors reviewed the manuscript.

References

1. Hayer-Hartl, M., Bracher, A., and Hartl, F. U. (2016) The GroEL-GroES chaperonin machine: a nano-cage for protein folding. *Trends Biochem. Sci.* **41,** 62–76
2. Saibil, H. R., Fenton, W. A., Clare, D. K., and Horwich, A. L. (2013) Structure and allostery of the chaperonin GroEL. *J. Mol. Biol.* **425,** 1476–1487
3. Sharma, S., Chakraborty, K., Müller, B. K., Astola, N., Tang, Y. C., Lamb, D. C., Hayer-Hartl, M., and Hartl, F. U. (2008) Monitoring protein conformation along the pathway of chaperonin-assisted folding. *Cell* **133,** 142–153
4. Lin, Z., Madan, D., and Rye, H. S. (2008) GroEL stimulates protein folding through forced unfolding. *Nat. Struct. Mol. Biol.* **15,** 303–311
5. Chaudhuri, T. K., Verma, V. K., and Maheshwari, A. (2009) GroEL assisted folding of large polypeptide substrates in *Escherichia coli*: present scenario and assignments for the future. *Prog. Biophys. Mol. Biol.* **99,** 42–50
6. Wood, S. J., Wypych, J., Steavenson, S., Louis, J. C., Citron, M., and Biere, A. L. (1999) α-Synuclein fibrillogenesis is nucleation-dependent. Implications for the pathogenesis of Parkinson's disease. *J. Biol. Chem.* **274,** 19509–19512
7. Selkoe, D. J. (1997) Alzheimer's disease: genotypes, phenotypes, and treatments. *Science* **275,** 630–631
8. Jacobson, D. R., and Buxbaum, J. N. (1991) Genetic aspects of amyloidosis. *Adv. Hum. Genet.* **20,** 69–123
9. Lu, J. X., Qiang, W., Yau, W. M., Schwieters, C. D., Meredith, S. C., and Tycko, R. (2013) Molecular structure of β-amyloid fibrils in Alzheimer's disease brain tissue. *Cell* **154,** 1257–1268
10. Ohi, T., Nabeshima, K., Kato, S., Yazawa, S., and Takechi, S. (2004) Familial amyotrophic lateral sclerosis with His46Arg mutation in Cu/Zn superoxide dismutase presenting characteristic clinical features and Lewy body-like hyaline inclusions. *J. Neurol. Sci.* **225,** 19–25
11. Uversky, V. N. (2008) Amyloidogenesis of natively unfolded proteins. *Curr. Alzheimer. Res.* **5,** 260–287
12. Uversky, V. N., Oldfield, C. J., Midic, U., Xie, H., Xue, B., Vucetic, S., Iakoucheva, L. M., Obradovic, Z., and Dunker, A. K. (2009) Unfoldomics of human diseases: linking protein intrinsic disorder with diseases. *BMC Genomics* **10,** Suppl. 1, S7
13. Knight, S. D., Presto, J., Linse, S., and Johansson, J. (2013) The BRICHOS domain, amyloid fibril formation, and their relationship. *Biochemistry* **52,** 7523–7531
14. Mainz, A., Peschek, J., Stavropoulou, M., Back, K. C., Bardiaux, B., Asami, S., Prade, E., Peters, C., Weinkauf, S., Buchner, J., and Reif, B. (2015) The chaperone αB-crystallin uses different interfaces to capture an amorphous and an amyloid client. *Nat. Struct. Mol. Biol.* **22,** 898–905
15. Wacker, J. L., Zareie, M. H., Fong, H., Sarikaya, M., and Muchowski, P. J. (2004) Hsp70 and Hsp40 attenuate formation of spherical and annular polyglutamine oligomers by partitioning monomer. *Nat. Struct. Mol. Biol.* **11,** 1215–1222
16. Shorter, J., and Lindquist, S. (2008) Hsp104, Hsp70 and Hsp40 interplay regulates formation, growth and elimination of Sup35 prions. *EMBO J.* **27,** 2712–2724
17. Klucken, J., Shin, Y., Masliah, E., Hyman, B. T., and McLean, P. J. (2004) Hsp70 reduces α-synuclein aggregation and toxicity. *J. Biol. Chem.* **279,** 25497–25502
18. Nishida, N., Yagi-Utsumi, M., Motojima, F., Yoshida, M., Shimada, I., and Kato, K. (2013) Nuclear magnetic resonance approaches for characterizing interactions between the bacterial chaperonin GroEL and unstructured proteins. *J. Biosci. Bioeng.* **116,** 160–164
19. Yagi-Utsumi, M., Kunihara, T., Nakamura, T., Uekusa, Y., Makabe, K., Kuwajima, K., and Kato, K. (2013) NMR characterization of the interaction of GroEL with amyloid β as a model ligand. *FEBS Lett.* **587,** 1605–1609
20. Noi, K., Kitamura, A., Hirai, H., Hongo, K., Sakurai, T., Mizobata, T., and Kawata, Y. (2012) Suppression of Sup35 amyloid fibril formation by group II chaperonin from *Thermoplasma acidophilum*. *Am. J. Mol. Biol.* **2,** 265–275
21. Ojha, B., Fukui, N., Hongo, K., Mizobata, T., and Kawata, Y. (2016) Suppression of amyloid fibrils using the GroEL apical domain. *Sci. Rep.* **6,** 31041
22. Machida, K., Fujiwara, R., Tanaka, T., Sakane, I., Hongo, K., Mizobata, T., and Kawata, Y. (2009) Gly192 at hinge 2 site in the chaperonin GroEL plays a pivotal role in the dynamic apical domain movement that leads to GroES binding and efficient encapsulation of substrate proteins. *Biochim. Biophys. Acta* **1794,** 1344–1354
23. Darby, N. J., and Creighton, T. E. (1993) *Protein Structure: In Focus*, IRL Press at Oxford University Press, Oxford, UK
24. Sakane, I., Hongo, K., Motojima, F., Murayama, S., Mizobata, T., and Kawata, Y. (2007) Structural stability of covalently linked GroES heptamer: advantages in the formation of oligomeric structure. *J. Mol. Biol.* **367,** 1171–1185
25. Shammas, S. L., Waudby, C. A., Wang, S., Buell, A. K., Knowles, T. P., Ecroyd, H., Welland, M. E., Carver, J. A., Dobson, C. M., and Meehan, S. (2011) Binding of the molecular chaperone αB-crystallin to Aβ amyloid fibrils inhibits fibril elongation. *Biophys. J.* **101,** 1681–1689
26. Kulig, M., and Ecroyd, H. (2012) The small heat-shock protein αB-crystallin uses different mechanisms of chaperone action to prevent the amorphous versus fibrillar aggregation of α-lactalbumin. *Biochem. J.* **448,** 343–352
27. Hochberg, G. K., Ecroyd, H., Liu, C., Cox, D., Cascio, D., Sawaya, M. R., Collier, M. P., Stroud, J., Carver, J. A., Baldwin, A. J., Robinson, C. V., Eisenberg, D. S., Benesch, J. L., and Laganowsky, A. (2014) The structured core domain of αB-crystallin can prevent amyloid fibrillation and associated toxicity. *Proc. Natl. Acad. Sci. U.S.A.* **111,** E1562–E1570
28. Glover, J. R., and Lindquist, S. (1998) Hsp104, Hsp70, and Hsp40: a novel chaperone system that rescues previously aggregated proteins. *Cell* **94,** 73–82
29. Dedmon, M. M., Christodoulou, J., Wilson, M. R., and Dobson, C. M. (2005) Heat shock protein 70 inhibits α-synuclein fibril formation via preferential binding to prefibrillar species. *J. Biol. Chem.* **280,** 14733–14740
30. Kitamura, A., Kubota, H., Pack, C. G., Matsumoto, G., Hirayama, S., Takahashi, Y., Kimura, H., Kinjo, M., Morimoto, R. I., and Nagata, K. (2006) Cytosolic chaperonin prevents polyglutamine toxicity with altering the aggregation state. *Nat. Cell Biol.* **8,** 1163–1170
31. Tam, S., Geller, R., Spiess, C., and Frydman, J. (2006) The chaperonin TRiC controls polyglutamine aggregation and toxicity through subunit-specific interactions. *Nat. Cell Biol.* **8,** 1155–1162
32. Shahmoradian, S. H., Galaz-Montoya, J. G., Schmid, M. F., Cong, Y., Ma, B., Spiess, C., Frydman, J., Ludtke, S. J., and Chiu, W. (2013) TRiC's tricks inhibit huntingtin aggregation. *Elife* **2,** e00710
33. Yagi, H., Kusaka, E., Hongo, K., Mizobata, T., and Kawata, Y. (2005) Amyloid fibril formation of α-synuclein is accelerated by preformed amyloid seeds of other proteins: implications for the mechanism of transmissible conformational diseases. *J. Biol. Chem.* **280,** 38609–38616

34. Lanzetta, P. A., Alvarez, L. J., Reinach, P. S., and Candia, O. A. (1979) An improved assay for nanomole amounts of inorganic phosphate. *Anal. Biochem.* **100,** 95–97
35. Kubo, T., Mizobata, T., and Kawata, Y. (1993) Refolding of yeast enolase in the presence of the chaperonin GroE: the nucleotide specificity of GroE and the role of GroES. *J. Biol. Chem.* **268,** 19346–19351
36. Xu, Z., Horwich, A. L., and Sigler, P. B. (1997) The crystal structure of the asymmetric GroEL-GroES-(ADP)7 chaperonin complex. *Nature* **388,** 741–750
37. Pettersen, E. F., Goddard, T. D., Huang, C. C., Couch, G. S., Greenblatt, D. M., Meng, E. C., and Ferrin, T. E. (2004) UCSF Chimera–a visualization system for exploratory research and analysis. *J. Comput. Chem.* **25,** 1605–1612